Available online at www.sciencedirect.com
ScienceDirect
International Journal of Mass Spectrometry 268 (2007) 93–105
International Journal of Mass Spectrometry
www.elsevier.com/locate/ijms

A novel high-capacity ion trap-quadrupole tandem mass spectrometer

Andrew N. Krutchinsky [a,*], Herbert Cohen [b], Brian T. Chait [b,**]

[a] *Department of Pharmaceutical Chemistry, UCSF, MC 2280, Mission Bay, GH, Room S512F, 600 16th Street, San Francisco, CA 94158-2517, USA*
[b] *The Rockefeller University, New York, NY, USA*

Received 19 March 2007; received in revised form 6 June 2007; accepted 10 June 2007
Available online 26 June 2007

Abstract

We describe a prototype tandem mass spectrometer that is designed to increase the efficiency of linked-scan analyses by >100-fold over conventional linked-scan instruments. The key element of the mass spectrometer is a novel high ion capacity ion trap, combined in tandem configuration with a quadrupole collision cell and a quadrupole mass analyzer (i.e. a TrapqQ configuration). This ion trap can store $>10^6$ ions without significant degradation of its performance. The current mass resolution of the trap is 100–450 full width at half maximum for ions in the range 800–4000 *m*/*z*, yielding a 10–20 *m*/*z* selection window for ions ejected at any given time into the collision cell. The sensitivity of the mass spectrometer for detecting peptides is in the low femtomole range. We can envisage relatively straightforward modifications to the instrument that should improve both its resolution and sensitivity. We tested the tandem mass spectrometer for collecting precursor ion spectra of all the ions stored in the trap and demonstrated that we can selectively detect a phosphopeptide in a mixture of non-phosphorylated peptides. Based on this prototype instrument, we plan to construct a fully functional model of the mass spectrometer for detecting modification sites on proteins and profiling their abundances with high speed and sensitivity.

Keywords: High-capacity ion trap; Tandem mass spectrometer; High efficiency linked-scan analysis; Precursor ion; Neutral loss scans

1. Introduction

Detecting the presence of post-translational modifications on proteins and quantifying their abundance are prerequisites for understanding many biological processes [1–3]. Despite the availability of an array of techniques for the elucidation of post-translational modifications [4–6], their study continues to present a formidable analytical challenge. Mass spectrometry (MS) is playing an increasingly important role in such analyses because it provides a fast, sensitive means to specifically localize and characterize covalent modifications [7–9].

Among the most powerful of the current MS techniques for the analysis of protein modifications is the analysis of proteolytic peptide mixtures using a combination of liquid chromatography with tandem MS (MS/MS). The resulting MS/MS spectra identify candidates that bear particular modifications [see, e.g., 10, 11]. However, such analyses are complicated by difficulties in detecting the often relatively low abundance modified peptides that frequently co-elute with more abundant unmodified species [12]. Different purification schemes have been devised to enrich specifically modified peptides or proteins [11,13–15].

An alternative method for elucidating post-translational modifications employs a hypothesis driven MALDI multistage-MS approach [16]. Because this approach is not limited by the time constraints inherent to LC–MS analyses, a large number of peaks and hypotheses can be checked by collecting MS/MS spectra of every observed species as well as every species hypothesized to be present in the sample. Despite impressive successes, both techniques often yield fragmentation spectra of only a subfraction of the species present in the sample.

Ideally, we would like to increase the coverage of the analysis by performing tandem MS on every ion in the *m*/*z* range of the instrument. Currently, the only technique that approximates such an analysis is the linked-scan mode available in triple quadrupole, quadrupole–quadrupole time-of-flight, ion trap, and

* Corresponding author. Tel.: +1 415 476 1866; fax: +1 415 502 4690.
** Corresponding author at: The Laboratory of Mass Spectrometry and Gaseous Ion Chemistry, The Rockefeller University, New York, NY 10021, USA. Tel.: +1 212 327 8849; fax: +1 212 327 7547.
E-mail addresses: krutcha@picasso.ucsf.edu (A.N. Krutchinsky), chait@rockefeller.edu (B.T. Chait).

1387-3806/$ – see front matter © 2007 Elsevier B.V. All rights reserved.
doi:10.1016/j.ijms.2007.06.015

Table 1
Characteristic neutral losses and product ions that can be used to scan for precursor ions bearing specific modifications

Modification	Residues	Scan	Fragment	+/-ve	References
Phosphorylation of proteins	S, T	Neutral loss of 98 Da	H_2PO_3	+	[27,28]
	S, T, Y	Precursors of *m/z* 79	PO_3	−	[29,30]
	S, T, Y	Precursors of *m/z* 63	PO_2	−	[30]
	Y	Neutral loss of 80 Da	HPO_3	+	[31]
	Y	Precursors of *m/z* 216.045	Phosphotyrosine-specific immonium ion	+	[32]
Glycosylation of proteins	N	Precursor of *m/z* 163	Hex, hexose	+	[33]
	N	Precursor of *m/z* 204	HexNAc+, *N*-acetylhexosamine oxonium ion	+	[33–36,28]
	N	Precursors of *m/z* 366	Hex-HexNac	+	[33]
	N	Neutral loss of 162 Da	Manose	+	[33]
	S, T	Neutral loss of 203 Da	GlcNAc	+	[28,35]
Acetylation of proteins	K	Precursor of *m/z* 143	Immonium ion of acetyllysine	+	[37,38]
	R	Precursor of *m/z* 199	Immonium ion of acetylarginine	+	[37]
Methylation of proteins	K, R	Precursors of 46 71 *m/z*	Dimethyl-ammonium and *N*,*N*′-dimethyl-carbodiimidium	+	[39]
Mono- and di-methylation	K	Neutral loss of 59 Da		+	[39]
Tri-methylation			Tri-methylamine	+	[40]
Nitration of proteins	Y	Precursor of *m/z* 181.06	Immonium ion of mono- and di-nitrotyrosine	+	[41]
		Precursor of *m/z* 226		+	[41]
Glutathionation of proteins	C	Neutral loss of 129	Pyroglutamic acid	+	[42]

sector instruments [17–26,32]. However, instead of producing complete MS/MS fragmentation spectra of every species in the *m/z* range of the instrument, the technique produces only spectra of those precursor ions that generate a particular ion product or a particular neutral loss. Table 1 provides examples of characteristic neutral losses and product ions that can be used to detect and profile precursor ions bearing specific post-translational modifications.

The yield of specific ion fragments that signal the presence of particular modifications can be very different for different fragments. For example, the yield of ions at *m/z* 71 used to detect the dimethylarginine-containing peptides is typically just a few percent of the total ion fragmentation signal [39], whereas the ion arising from the facile neutral loss of 98 Da from serine- or threonine-phosphorylated peptides can dominate the fragmentation spectrum [28]. The *m/z* value of these characteristic 98 Da neutral loss fragments depends on the charge state of the peptide. Fragmentation of singly charged parent ion causes the appearance of characteristic fragment separated by 98 Da, whereas doubly or triply charged ions produce respectively the loss of 49 Da and 32.7 Da. Theoretically, similar mass reduction may occur when a peptide contains proline (M_W 97) or valine (M_W 99) at either of its termini. Practically, however, in the case of the tryptic digestion of proteins, the occurrence of proline at the N-terminus is rare because the digestion rate of the –RP– or –KP– bond is very low [43]. The gas phase hydrolysis of N-terminal valines also occurs at a low rate (personal observation). Thus, the loss of 98 provides an excellent signature for the specific presence of phosphorylation.

The duty cycle, and therefore the relative efficiency of linked-scan analysis, as currently performed, is extremely low when a wide precursor ion mass range is interrogated. As shown in Fig. 1A, every time we select a small window of precursor ions (e.g., 3–4 amu) for collision-induced dissociation, the rest of the ions in the spectrum (over a typical mass range of 3000–4000) are rejected, resulting in an efficiency of ∼0.001. These rejected ions are lost for subsequent analysis. In principle, we can significantly improve the efficiency of the linked-scan experiment

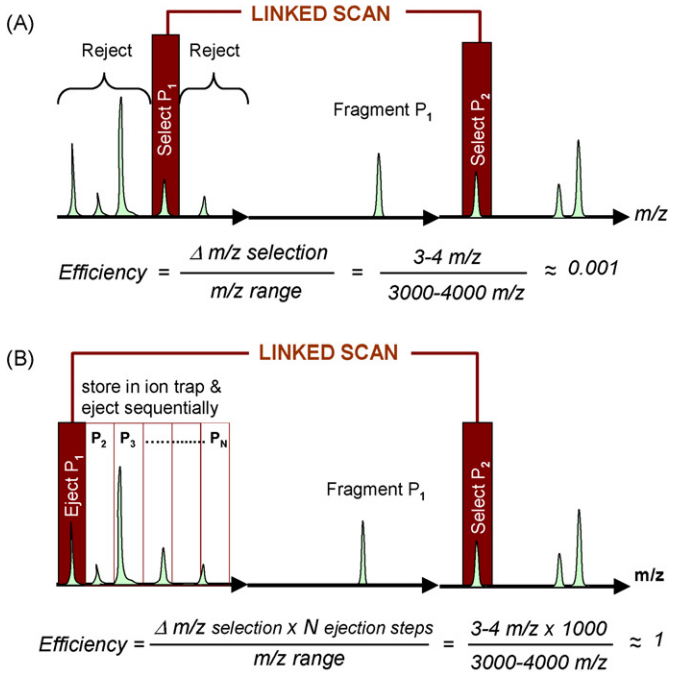

Fig. 1. (A) Representation of the major steps in a linked-scan analysis as currently performed using, for example, the triple quadrupole mass spectrometer. The efficiency is low (∼0.001) because the duty cycle of the experiment is low. (B) Representation of an improved scheme for linked-scan analysis using a tandem mass spectrometer consisting of an ion trap followed by a collision cell followed by a mass analyzer. Here, the efficiency can approach unity when all the ions stored in the trap are sequentially fragmented and analyzed.

if we configure a tandem mass spectrometer as an ion trap followed by collision cell followed by mass analyzer, i.e., a TrapqQ (Fig. 1B). In this configuration, we can utilize the ability of the ion trap to store all ions until we sequentially eject them using a resonant and/or instability scan [44]. Thus, after we fill the trap, we can eject ions sequentially as a function of *m*/*z* in packets of 3–4 *m*/*z*, while stably retaining the rest of the ions in the trap. We can then accelerate each packet of these ejected ions into a collision cell to perform collision-induced dissociation (CID). We can choose to detect only a particular ion fragment or the ion corresponding to a particular neutral loss in the mass analyzer that follows the collision cell. If we link the ion trap ejection scan with the detection of a particular fragment in the mass analyzer, we can produce a very efficient linked-scan mass spectrometer. The theoretical efficiency of such a linked-scan approach reaches unity because all ions stored in the ion trap can be subjected to such analysis, resulting in ~1000-fold improvement over efficiencies normally achieved in current instruments.

The realization of the above-described strategy will be limited in practice by the number of ions that can be trapped during any one cycle of the instrument. For example, it has been estimated that the performance of conventional 3D ion traps (e.g., Finnigan LCQ) is degraded by space charge effects when the number of ions in the trap exceeds 10^3–10^4 [49]. These are too few ions to yield useful fragmentation statistics on more than just a small number of relatively high-abundance precursor ion species in a mixture. While one can increase the counting statistics by repeating the experiment many times, this improvement is achieved at the cost of greatly increasing the time of the experiment—since the ion filling time is usually very short (~ms) compared to the MS readout time (~s, see later). Thus, for the practical realization of the strategy shown in Fig. 1B, it is crucial to incorporate an ion trap with sufficiently high ion capacity—preferably, at least 1000-fold higher than conventional 3D traps.

We used these principles to design and construct a prototype high efficiency linked-scan mass spectrometer that incorporates a novel high ion capacity ion trap. We describe the theory that governs the operation of this ion trap, show computer simulations of ion trajectories in the device, and establish that the trap can store a large number of ions without significant degradation in the performance. We demonstrate that ions stored in the ion trap can be sequentially fragmented in the collision cell during the ejection process, and that only particular ion fragments are transmitted to the detector through the quadrupole mass analyzer when the analyzer scan is linked to the ion trap ejection scan. Thus, a linked scan spectrum can be obtained from all ions stored in the ion trap during a single scan of the instrument. Based on our results we propose to build a fully functional mass spectrometer that will operate in the linked scan mode with efficiencies 100–1000 times higher than those available in the current instruments.

2. Experimental

Fig. 2 is a schematic of the tandem mass spectrometer that we constructed at the Rockefeller University. The vacuum chambers were machined from 4 in. × 4 in. × 0.5 in. square section aluminum alloy tubing (Hadco Aluminum, NY) and connected in a T-shaped configuration through flanges with viton rings. The components of the instrument are discussed below:

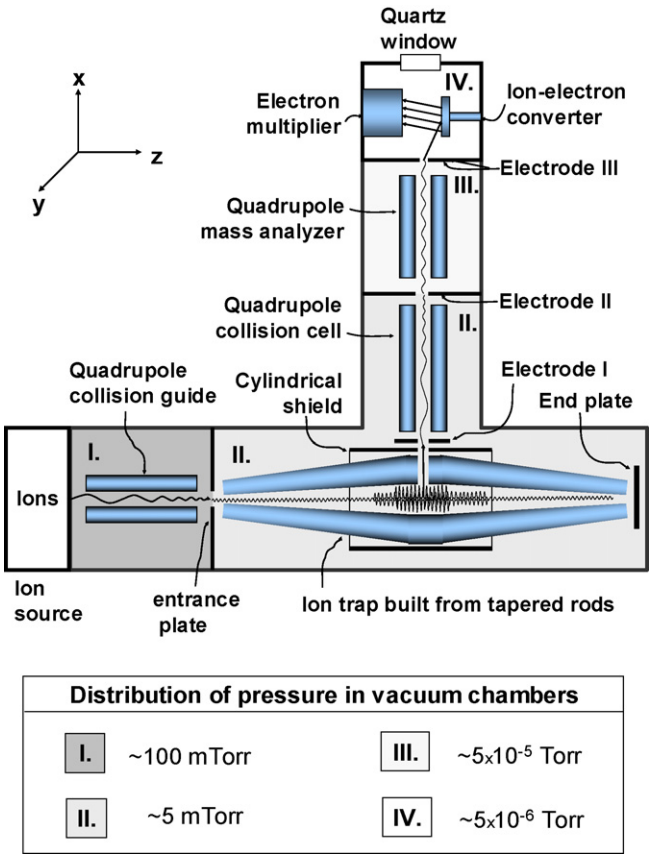

Fig. 2. Schematic of the TrapqQ tandem mass spectrometer. This instrument shows us to use the linked-scan scheme shown in Fig. 1B.

2.1. Ion source and laser system

The CD-MALDI ion source is similar to those that we have described previously [45,46]. Briefly, ions are produced by short duration (4 ns) pulses of 337 nm wavelength laser light (Nitrogen laser, VSL-337, Spectra Physics, Mountain View, CA) operating at a repetition rate of 1–20 Hz. The beam is reflected by a mirror, passed through a lens (f = 10 cm) and then through a quartz window to the surface of the CD at an angle of incidence of ~60°. The diameter of the laser spot on the sample surface is 0.3–0.5 mm. The power density of laser radiation in the spot can be varied in the range (1–5) × 10^7 W/cm^2 by changing the distance of the lens to the target. Both the sample and laser spot fluorescence are monitored by a video camera.

Desorbed ions are introduced directly into a quadrupole ion guide built from four cylindrical rods with diameter = 6.35 mm and length = 140 mm. The chamber is evacuated by a rotary pump (Edwards EM-12 4.7 L/s). The pressure of the air in the chamber is maintained at 70 mTorr by a variable leak valve. The quadrupoles of the ion guide, collision cell and mass analyzer are each driven by an independent RF power supply, consisting of a 500 kHz crystal oscillator-controlled sine wave generator,

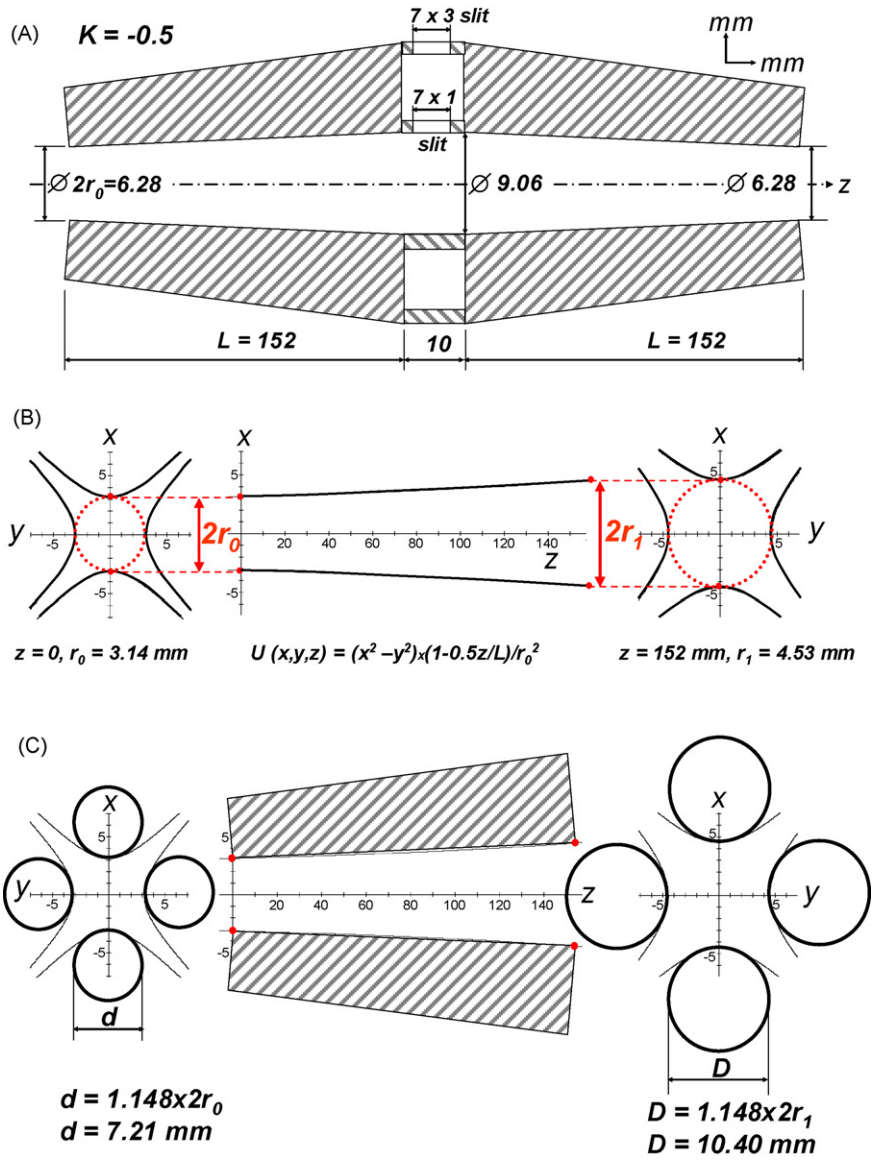

Fig. 3. (A) Schematic of the novel high ion capacity ion trap with dimensions indicated. (B) Geometry of quadrupoles that create the field $U(x, y, z)$ described by the equations provided in the figure. The acuteness of the hyperbola changes from the one end of the ion trap, $z = 0$, to its middle, $z = 152$ mm; the distance between the opposing hyperbola changes approximately linearly from 6.28 mm to 10.06 mm. Parameter $k = -0.5$. (C) The potential shown in (B) can be approximated using tapered rods. For best approximation, the optimum diameter of the rods is 1.148 times the distance between opposing rods.

a power amplifier and a RF transformer, all designed and constructed in-house. The typical amplitude of the RF voltage is 250–500 V. Details on the circuitry are described elsewhere [46].

2.2. Novel high-capacity ion trap

The ion trap was constructed from eight stainless steel (SS) tapered rods and four SS tubes connecting these tapered rods, as shown in Fig. 3A together with their dimensions. We purchased a number of standard pre-fabricated tapered rods (taper pins #7, ANSI standard, McMaster-Carr, USA), and sorted these for consistency of the desired dimensions, i.e., small end diameter 0.284 in. (7.21 mm), large end diameter 0.409 in. (10.4 mm), length 6 in. (152 mm). Both values of small and large diameters determine the parameter k in Eq. (2) below to be very close to −0.5. The central part of the ion trap is enclosed by a SS cylinder with internal diameter 31.75 mm (1.25 in.), outside diameter 34.9 mm (1.375 in.) and the length of 50.8 mm (2 in.) (Fig. 2) so as best to approximate a quadrupole field [47].

The ion trap is driven by an independent RF power supply, wherein the main RF frequency is fixed at 333 kHz. A secondary low voltage resonance ejection RF is applied to one pair of the rods as shown schematically in Fig. 5. The amplitude of the main RF voltage is maintained at 100 V for a specified time period, usually 1 s, during which time the trap is filled with ions that pass through the quadrupole ion guide. After 1 s, the main RF amplitude is ramped to 600 V at a rate of 500 V/s. The amplitude of the resonant ejection RF is ramped in phase with the main RF at values that are typically in the range 1–6 V. The frequency and amplitude of the resonant ejection RF are set

using a DS345 function arbitrary waveform generator (Stanford Research Systems, Sunnyvale, CA). The action of these time varying potentials cause ions to be ejected sequentially as a function of mass through a slit (1 mm × 7 mm) in one of the connecting quadrupole rods (Fig. 3A). These ejected ions then enter the collision cell of the tandem instrument.

2.3. Quadrupole collision cell

The entrance of the collision cell is close to and aligned with the output slit of the trap (Fig. 2). This quadrupole collision cell is built from rods with diameter = 10 mm and length = 300 mm. The quadrupoles are driven in the RF only mode by a 500 kHz power supply. Both the trap and the collision cell are evacuated by a 250 L/s turbo pump (Turbo V-250 Varian). The pressure in the trap and collision cell chambers is regulated through a controllable leak valve connected to a He gas cylinder. In this way, the operating pressure in the trap can be varied in the range 0.1–10 mTorr. We determined experimentally that the optimal pressure of He in this chamber is 2–5 mTorr. Currently, the collision cell and ion trap are not isolated from one another with respect to gas flow, and therefore they can only operate under conditions where both are filled with the same gas at the same pressure. Modifications are underway to allow us to use different pressures of different gases in the ion trap and in the collision cell, so as to be able to optimize CID in the collision cell without affecting trapping and ejection from the ion trap.

2.4. Quadrupole mass analyzer

Here, we utilized a quadrupole from a retired triple quadrupole instrument (TSQ 700, Finnigan), which has four hyperbolic shaped rods of length 160 mm and the distance between opposing rods is 8 mm. It is positioned in a compartment adjacent to the collision cell (Fig. 2), which is evacuated by a separate 250 L/s turbo pump (Turbo V-250 Varian) to a pressure $\sim 5 \times 10^{-5}$ Torr. The quadrupole operates either in an RF only mode or a mass filter mode. A 500 kHz power supply (constructed in-house) drives the quadrupoles in the RF only mode (0–700 V). To operate it as a mass filter, we apply a DC voltage of up to ±(0–100) V to opposite pairs of the quadrupole. In the present prototype mass spectrometer, we selected peaks by manual adjustment of these RF and DC voltage amplitudes [47].

2.5. Detector

The detector consist of an ion-to-electron converter (−10 kV) and an electron multiplier (5903 Magnum Electron Multiplier, Burle, Lancaster, PA). Ion signals are amplified by a low-noise current preamplifier (SR570 Stanford Research Systems, Sunnyvale, CA) and applied to a LeCroy digital oscilloscope (Model 9310A, LeCroy Corporation, USA), triggered by the start of the ramping process. All spectra reported in this paper were taken with a digital camera directly from the screen of the oscilloscope. The detector vacuum chamber is evacuated by a third 250 L/s turbo pump (Turbo V-250 Varian) to the pressure $\sim 10^{-6}$ Torr.

2.6. Ion optics

DC voltages to all elements of the ion optics of the instrument is provided by an in-house constructed multi-channel power supply. The values of the DC voltages on the ion optical elements (Fig. 2) are—MALDI target +200 V [46], offset of quadrupole collision guide: +20 V, ion trap entrance and end plates: +10 V, the trap: 0 (grounded), electrode I: from 0 up to −2000 V, offset of quadrupole collision cell: −10 V, electrode II: −15; offset of the quadrupole mass analyzer −20, electrode III: −25 V, ion-to-electron converter −10 kV, electron multiplier −1600 V.

2.7. Samples and sample preparation

A stock mixture of Substance P (1346.7 Da), neurotensin (1671.9 Da), amyloid β-protein fragment 12–28 (1954.0 Da), ACTH fragment 1–24 (2931.6 Da), and insulin chain B, oxidized, from bovine insulin (3493.6 Da) was prepared at a concentration 200 fmol/μL per component in water/methanol/acetic acid (35/60/5, v/v/v). A small aliquot of the mixture was mixed with a saturated solution of 2,5-dihydroxybenzoic acid matrix (Sigma–Aldrich) and deposited on the surface of a compact disk (CD) MALDI target [46]. We used the synthetic phosphopeptide GRTGRRNpSIHDIL *m/z* 1574.8 to test the precursor scan mode of the tandem instrument.

2.8. Computer programs

We simulated the ion motion inside the ion trap using a program written in-house (LabVIEW graphical programming language version 7, National Instruments, Austin, TX) on a PC computer.

3. Theory

Detection of post-translational modifications by the linked-scan procedure requires that the modified species generate a specific "signature" fragment upon CID (Table 1). Currently available instruments [17–26] are very inefficient for such linked-scan analyses (Fig. 1A). As discussed above, in theory we can improve this efficiency by up to 1000-fold using a tandem mass spectrometer assembled in the TrapqQ configuration shown in Fig. 1B. A key element in achieving this improvement is the production of an ion trap that is capable of storing a large number of ions and ejecting these ions sequentially as a function of mass. Here, we consider the design of such an ion trap.

3.1. Ion storage capacity considerations

We will make a case here that a conventional 3D trap is not suitable for our proposed tandem instrument. The major parameter that limits the rate of a linked scan in the TrapqQ instrument is the time that ions spent in the collision cell. We estimate this time from the typical values that are used in linked scan experiments performed in triple quadrupole instruments [19,20]. A

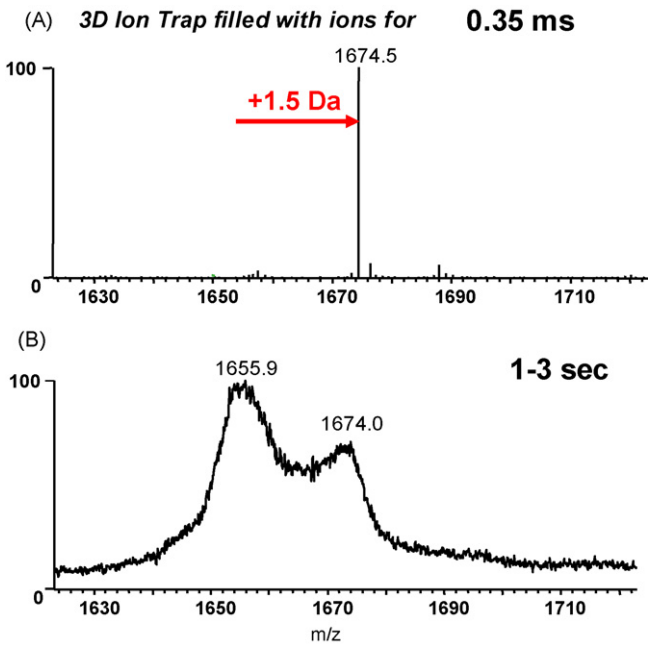

Fig. 4. MALDI mass spectra of a 100 fmol sample of a peptide at *m/z* 1673 obtained for different ion injection times into a 3D ion trap [46]: (A) 0.35 ms and (B) 3 s.

minimum time of ~1 ms is needed to fragment an ejected packet of ions, to cool these fragments, and to pass them downstream to a mass analyzer without interference from fragments of previously ejected ions (i.e., to avoid crosstalk). Thus, if we eject and analyze a 4 *m/z* portion of ions every millisecond, we need ~1 s to perform a linked scan analysis over a range of 4000 *m/z*. To achieve high efficiency, we need to inject ions into the ion trap for a comparable period of time, i.e., ~1 s. Fig. 4 illustrates what happens to the performance of an ordinary 3D ion trap when we fill it with ions from a MALDI ion source [46] for increasing periods of time. The rate of ions produced in the MALDI source from a 100 fmol peptide sample is sufficient to overfill the trap, even in the shortest fill-in time (0.35 ms) that could be set on a commercial instrument. The *m/z* of the peptide peak (1674.5) is shifted by more than 1 Da from its correct value (1672.9 *m/z*), which is a typical sign of space charge effects (Fig. 4A). Such peak shifting effects are observed when the ion count in the 3D ion trap exceeds 10^3–10^4 ions [48–49]. When we fill the ion trap for 3 s at 10 Hz laser frequency, for all practical purposes it ceases to operate as a mass spectrometer. Instead of a single sharp ion peak at the appropriate mass, it produces broad humps spanning masses that are not readily related to the peptide mass (Fig. 4B). Further increasing the fill time to 3–10 s at the same laser frequency (10 Hz) causes coalescence of broad peaks into one very sharp peak at an incongruous mass [50]. Such curious phenomena arise when ion traps are filled with the order of 10^6–10^8 ions.

A number of alternative geometries have been devised to improve the ion storage [51–57]. Improvements in the performance of linear ion traps operating with 30–50 times more ions than "standard" 3D ion traps have been attributed to their increased ion storage capacity [55,56]. Here, we demonstrate that we can achieve even higher ion storage capacities using a new ion trap design.

3.2. Operating principle of the new ion trap

The new ion trap is composed of two non-linear quadrupole arms each composed of four tapered rods, joined at their widest ends by a short linear quadrupole (Fig. 3A). We call this configuration the "dual tapered ion trap". The purpose of this configuration is to create in each non-linear quadrupole arm an electric potential that closely approximates

$$U(x, y, z) = U_0 \left(\frac{x^2 - y^2}{R^2} \right) + C \tag{1}$$

where

$$R = \frac{r_0}{\sqrt{1 + kz/L}} \tag{2}$$

This potential satisfies the Laplace's equation ($\Delta U = 0$), where the constants U_0, r_0, L, k and C are determined from particular initial and boundary conditions. The parameters describing the particular geometry of our trap are provided in Fig. 3.

Eq. (1) closely resembles the potential of a linear quadrupole, except that the field radius R scales as a function of z according to Eq. (2). Fig. 3B indicates the dimensions of hyperbolic rods that can be used to approximate the potential given by Eqs. (1)

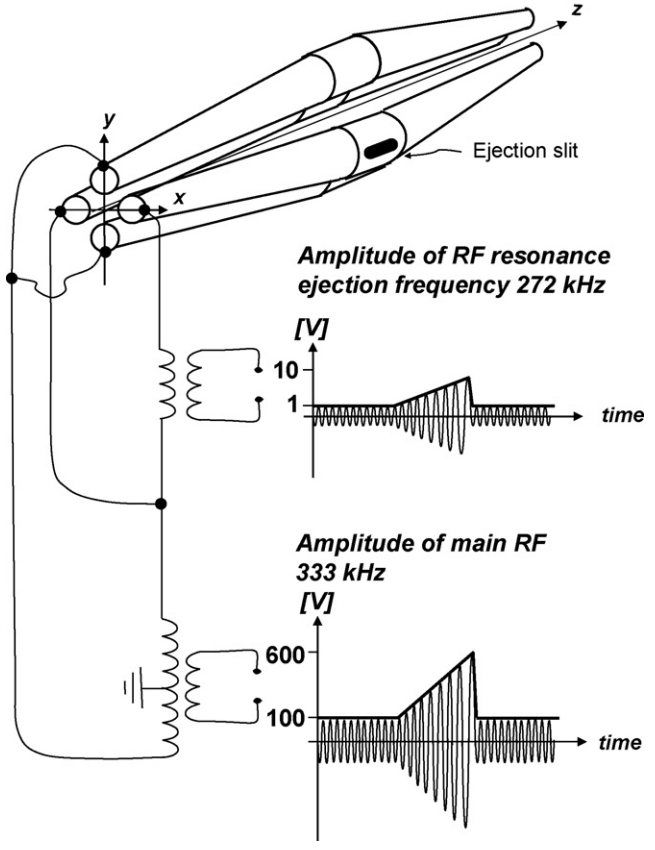

Fig. 5. Schematic of the dual tapered rod ion trap showing the applied RF voltages.

and (2). Note that the acuteness of the hyperbola changes from one end of the tapered rods to the other and the distance between the rods changes approximately linearly. For practical reasons, we chose to use round tapered rods instead of hyperbolic tapered rods to produce a potential that approximates that described by Eqs. (1) and (2). For best approximation of a quadrupole potential, the diameter of the rods is set at 1.148 of the distance between rods (i.e., the diameter of the field) [47] (Fig. 3C).

When a radio frequency (RF) voltage is applied to the dual tapered ion trap (Fig. 5), it creates time-varying electrical fields that trap ions inside the device. Analysis of ion motion in the potential given by Eqs. (1) and (2) is rather complicated [47]. For illustrative purposes, it is easier to consider the ion motion in a time-averaged effective potential [47,58], the approximate shape of which is shown in Fig. 6A. It is seen that the walls of the parabolic potential are steeper at the ends of the trap and shallower towards the center. This results in an effective force along the z-coordinate, directed towards the center of the ion trap. The magnitude of this force is directly proportional to the distance between the ion and the z-axis (Fig. 6B).

Motion of ions in such an effective potential is influenced by the components of a force along all three coordinates as well as collisions with gas molecules. As ions collide with molecules of buffer gas they gradually loose their kinetic energy and accumulate at the bottom of the potential well [59,60]. Since the force along the z-coordinate is negligible at the bottom of the well, ions will eventually spread along the entire z-axis under the influence

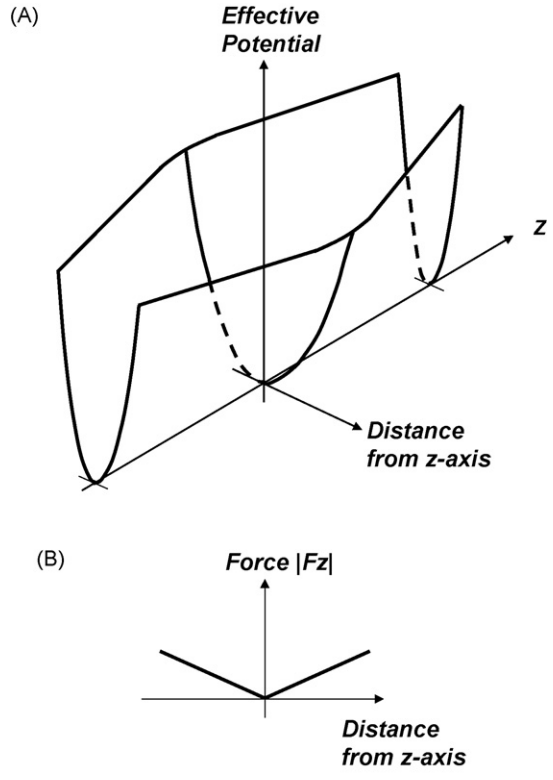

Fig. 6. (A) Approximate shape of an effective potential created in the dual tapered rod ion trap. (B) The magnitude of the force along the z-coordinate that pushes ions towards the central part of the ion trap is proportional to the distance between the ion and the z-axis.

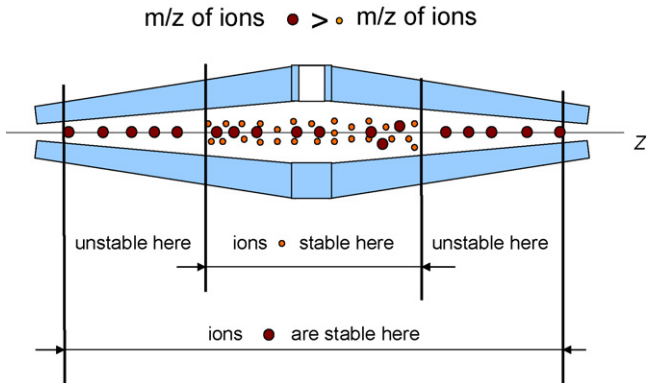

Fig. 7. Schematic illustration of the areas of stability for ions with two different m/z values at a particular amplitude of the RF voltage. Further increasing the RF amplitude during the ramping process moves the excitation boundaries inwards.

of the repulsive space charge forces between ions in the trap. To prevent escape of ions from the trap, small potentials are applied to the entrance and end plates (Fig. 2).

After ions fill the entire ion trap, the ejection process starts by ramping up the amplitude of RF voltage of the main driving frequency and the dipolar resonance frequency applied to the rods (Fig. 5). This is a standard way to eject ions from ion traps [44,55]. What is non-standard for this particular ion trap is that ions positioned close to ends of the ion trap with the lowest m/z values, become excited first [47]. Under these conditions, the amplitude of the ion oscillation along the y-coordinate increases when we apply a dipolar excitation signal to the pair of rods in (xz)-plane, as illustrated in Fig. 5. This increased oscillation amplitude, in turn, causes an increase in the force along the z-coordinate—driving ions towards the center of the trap. As the RF voltage amplitudes increase further, the excitation region moves inwards, concentrating the ions of particular m/z at the center of ion trap (Fig. 7). Interestingly, ions having larger m/z values remain unaffected by these RF voltages until their amplitudes grow sufficiently high to begin to induce their excitation in the ion trap. Thus, ions of each m/z value are sequentially compressed by a "wave" of excitation towards the center of ion trap, where they are eventually ejected through a small slit made in one of the rods. We verified this principle of ion ejection using computer simulations of ion motion in the dual tapered ion trap.

4. Calculations

We wrote a computer program to simulate ion motion in the trap based on a Monte Carlo model [59], utilizing the equation for a "perfect" electrical field (1) and (2) in each tapered quadrupole arm of the device.

Fig. 8(A) shows typical projections of an ion trajectory on the (xz)-plane. The simulation illustrates the behavior of trajectories for an ion with m/z 1673 as we ramp upwards the amplitudes of the main driving and dipolar excitation frequencies. The initial parameters for these simulations were chosen to be close to the experimental values (Fig. 3). Analysis of the simulated trajectories clearly shows the spatial compression of ion tra-

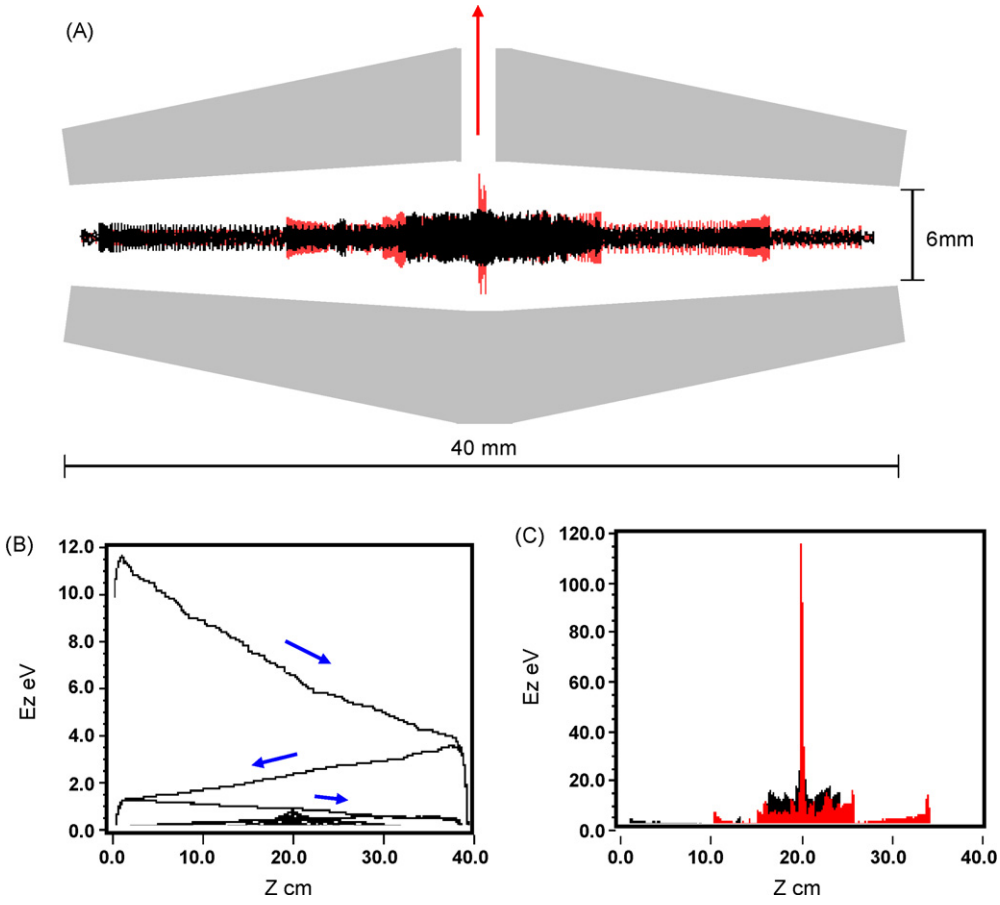

Fig. 8. (A) Simulation of ion trajectories in the dual tapered rod ion trap using the "ideal" field given by Eqs. (1) and (2). Projections of the trajectory of one ion with *m*/*z* 1673 are shown in two different colors: red is the projection onto the (*xz*) plane and black that onto (*yz*) plane. Bunching of trajectories at the central part of the trap indicates ion compression through ramping the RF voltage amplitude. The values used for the dimensions of the ion trap and voltages applied to it are given in Figs. 3 and 5. The collision gas is He at a pressure of 4 mTorr. (B) The ion gradually loses its kinetic energy in collisions with the He gas while moving back and forth along the ion trap. Arrows indicate the direction of ion motion. (C) The behavior of the radial component of the ion energy during the ramping process. The ion is ejected in the middle of the trap with a kinetic energy 120 eV.

jectories during the ion ejection process. As the amplitudes of both the main RF and excitation RF increase, the ion becomes excited at the inward moving stability boundaries, i.e., excitation "waves" compress ions towards the central part of the trap (Fig. 8A). The component of the ion energy along the *z*-axis gradually decreases due to collisional cooling as the ion moves backwards and forwards between the entrance and the end plates (Fig. 2). The radial oscillation of the ion in the (*xz*)-plane and (*yz*)-plane increases until the ion has sufficient energy to overcome the effective potential of the well, whereupon the ion is ejected (Fig. 8C).

Simulations performed with this program showed that ions of different *m*/*z* are sequentially compressed and ejected from the trap under a wide variety of initial conditions, including the amplitude and frequency of the RF fields and the pressure and type of collision gas. One interesting feature of the trap is that it can simultaneously trap positive and negative ions. Our simple computational model allowed us to confirm the basic principles of operation of our novel dual tapered ion trap, and helped us to choose the parameters for a particular configuration, which we built and tested experimentally.

5. Results

5.1. Mass spectrum of a peptide mixture

Fig. 9A shows the mass spectrum of a five-peptide mixture (100 fmol of each component) obtained in a single 1 s-scan of the tandem instrument depicted in Fig. 2. Let us briefly describe the sequence of the events during the acquisition of such a spectrum.

To produce MALDI ions, we irradiate the sample with laser pulses at a repetition rate of 1 Hz. The produced ions are cooled in the quadrupole collision ion guide operated in RF-only mode (Fig. 2), and then enter the dual tapered trap operating in the fill mode, i.e., where the amplitude of the main RF (333 kHz) voltage is ~100 V, and the amplitude of excitation RF (272 kHz) is ~1 V. After a 1 s fill, we start to ramp up the amplitudes of both the main RF voltage and the excitation RF voltage at rates of ~500 V/s and ~5 V/s, respectively (Fig. 5). Ions ejected through the slit in the ion trap pass the collision cell and the quadrupole mass analyzer and are detected (see Fig. 2). The start of the ramping process triggers a digital oscilloscope that records the ion spectrum.

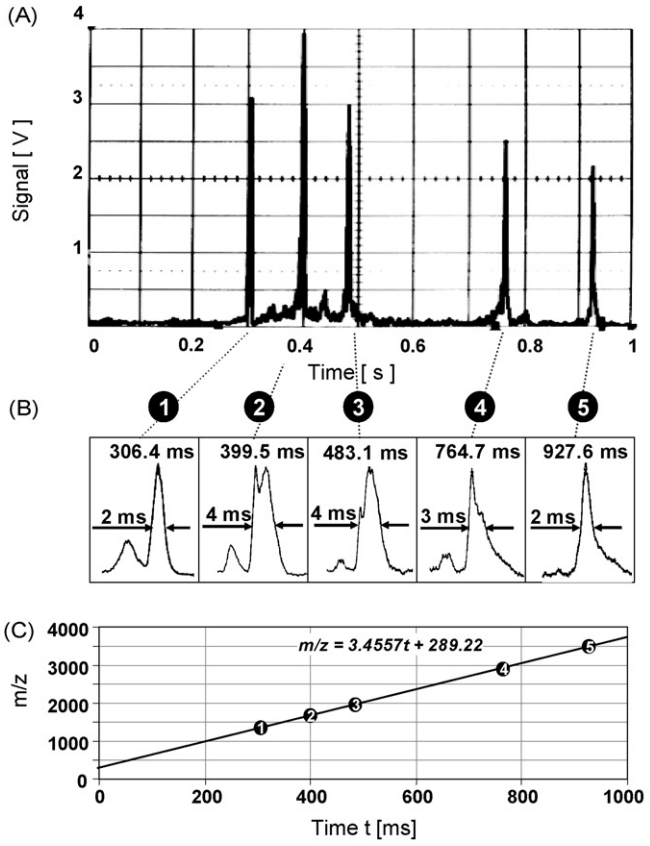

Fig. 9. (A) MALDI time (mass) spectrum obtained from a five-peptide mixture (100 fmol of each) measured in a single 1 sec-scan of the tandem instrument. Repetition rate of the laser was 1 Hz. (B) Detail showing width and the shape of the ion peaks. (C) Mass calibration curve.

Empirically, we found the optimum frequency of the resonance ejection to be 272 kHz, a value that provided the best combination of resolution, sensitivity and the *m/z* range of the ion trap. Ejection occurred efficiently only at "islands" around particular frequencies, which probably correspond to non-linear resonances arising from the imperfect fields that approximate Eqs. (1) and (2). The resolution of the ion trap (convoluted with the time-of-flight spread of ions in the collision cell) was 100–450 (Fig. 9B), corresponding to a width of ~10–20 Da at half maximum. Calibration of the ion trap yielded the expected linear dependence between the ejection time and *m/z* of the ejected ions (Fig. 9C).

5.2. Sensitivity of the ion trap

The signals from the samples containing 100 fmol, 10 fmol and 1 fmol of each peptide were detected after a single 1 s scan of the ion trap and essentially a single laser shot because the laser was operated at 1 Hz (Fig. 10). We attribute this high sensitivity to the large number of ions that can be stored in the ion trap.

5.3. Number of ions in the dual tapered trap

To estimate the number of ions stored in the dual tapered trap, we directly compared the amplitudes of signals produced

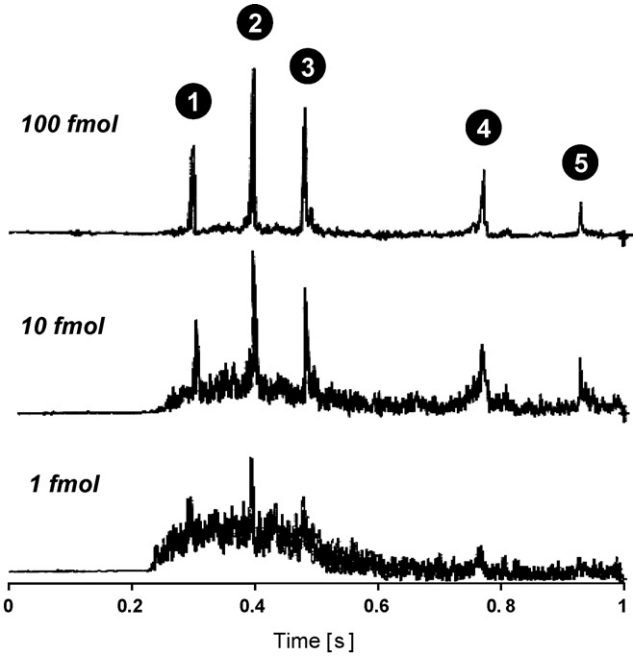

Fig. 10. MALDI time spectra obtained from 100 fmol, 10 fmol and 1 fmol samples of a five-peptide mixture measured in a single 1 s-scan of the tandem instrument. Repetition rate of the laser was 1 Hz.

by single ions and by ions from a peptide sample. To produce single ions, we illuminated an ion-electron converter with a UV light (UV lamp ENF-260C, Spectroline, Westbury, NY) introduced through the quartz window into the compartment of the detector assembly (see Fig. 2). Fig. 11A shows several single-count events generated by the UV light. The average amplitude of a single-ion event was about 50 mV at the 5 nA/V gain of the amplifier. The average amplitude of the signal from the three peptide signals present in the spectrum was ~1.5V at the 5 μA/V

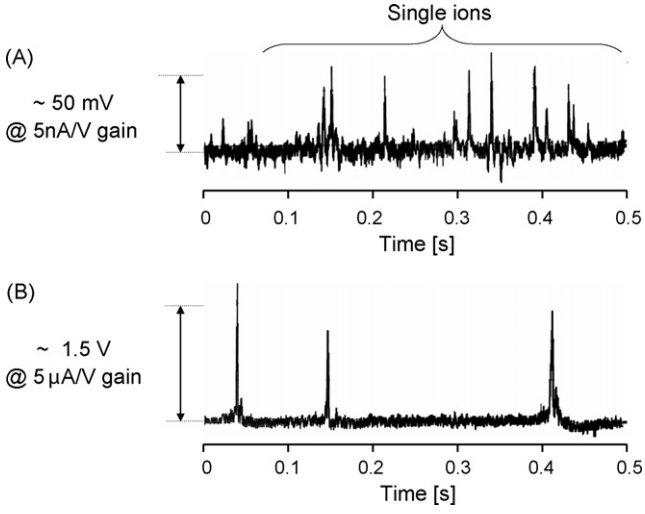

Fig. 11. (A) Typical amplitudes of single ions produced by a UV light source; amplifier gain = 5 nA/V. (B) Amplitude of signal from three peptides ejected from the dual tapered ion trap; amplifier gain = 5 μA/V. Note the scan time in this experiment was 0.5 sec.

gain of the same highly linear amplifier (Fig. 11B). In addition, we estimate that the signal from this peptide constitutes ~2.5% of total ion signal detected in the range of the mass spectrometer from 1000 *m*/*z* to 4000 *m*/*z*. This was estimated from the spectra measured in a MALDI-QqTOF mass spectrometer fitted with a similar CD-MALDI ion source, and which operating in ion counting mode [45]. Thus, we can calculate the approximate number of ions ejected from the ion trap in a single scan:

$$N \approx 40 \frac{1.5 \times 1000}{0.05} \approx 1,000,000$$

The number is likely to be even larger considering ion losses during transfer through the collision cell and quadrupole mass analyzer. The number of ions can be further increased by increasing the repetition rate of the MALDI laser beyond the 1 Hz used for these measurements. Indeed, as we increase the laser repetition rate to 20 Hz, thereby filling the trap with $>10^7$ ions, we observed interesting effects that we attribute to space charge problems (see below).

5.4. Space charge effects

Fig. 12A shows the effect of increasing the repetition rate of the laser from 1 Hz to 20 Hz. The signals from several peptides disappear in the spectrum of the 100 fmol peptide mixture. The first ions to disappear are those with the lowest *m*/*z* values. As we increase the repetition rate, ions with progressively higher *m*/*z* disappear from the spectrum, on occasion resulting in the detection of only the signal from the highest *m*/*z* species (insulin chain B peptide; *m*/*z* 3965).

We can abolish this effect by grounding the end plate electrode (Fig. 2), allowing ions to escape from this end of the tapered ion trap. Interestingly, under this condition, we still obtain a spectrum of the peptides (Fig. 12B), albeit with a lower total ion signal. This observation likely indicates that a significant proportion of ions are not cooled down completely by the collisions with the He gas, and have sufficiently large radial oscillations to be contained in the ion trap only by the dynamic component of the force along the *z*-coordinate. Under these conditions, we can restore the ion signal close to the original (i.e., obtained

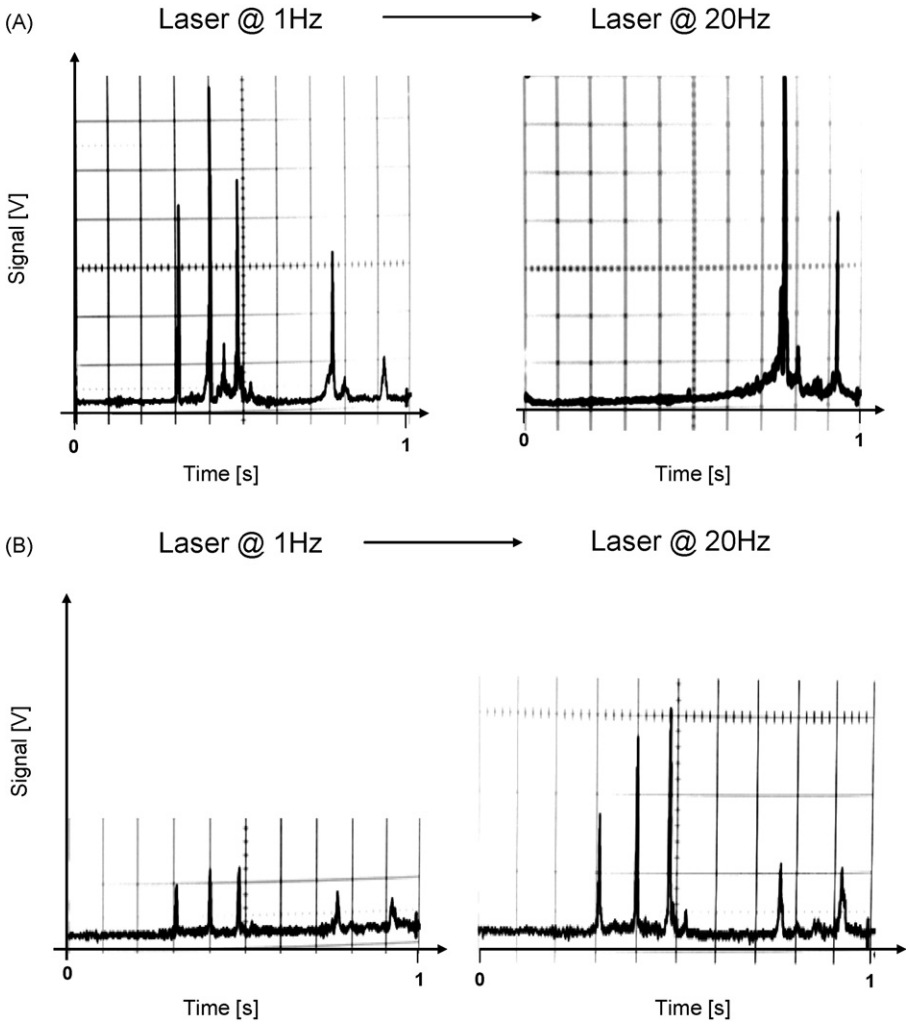

Fig. 12. (A) MALDI time (mass) spectra obtained from a five-peptide mixture (100 fmol of each) when the repetition rate of the laser was changed from 1 Hz to 20 Hz; end plate voltage = +10 V. (B) MALDI time (mass) spectra obtained under similar conditions to (A) and end plate voltage = 0 V.

at 1 Hz with trapping using a positive potential on the end plate) when the repetition rate of the laser is increased to 20 Hz. No space charging effects are observed under these condition. Apparently, the ion trap ejects the excess charge which otherwise interferes with its normal operation (although a detailed explanation of these phenomena will require further experimentation).

5.5. Precursor ion scan in the tandem mass spectrometer

We tested the performance of the tandem mass spectrometer in the precursor ion scan mode, i.e., the most straightforward linked-scan mode that we were able to readily reproduce in our instrument given our current rudimentary level of electronic control. Fig. 13A shows the spectrum of the previous five-peptide mixture, now spiked with 100 fmol of phosphopeptide. The signal of the phosphopeptide is marked in the spectrum with a star. We also detected a fragment, marked with an asterisk, originating from the loss of 98 Da. The yield of this fragment was deliberately increased in the MALDI process by increasing the laser pulse intensity 2–3-fold above the usual operating value.

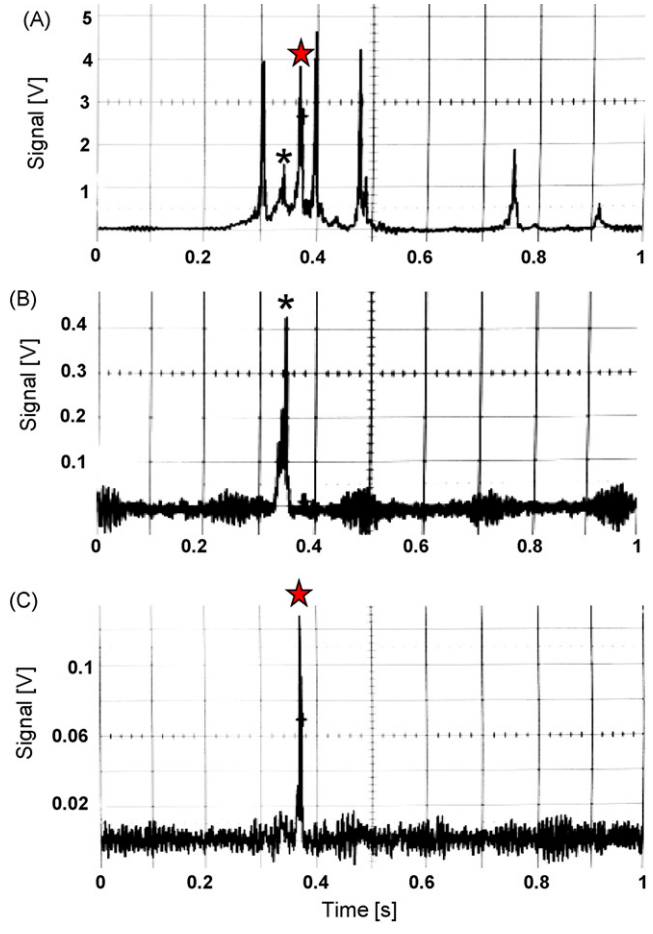

Fig. 13. (A) MALDI time (mass) spectrum obtained from a 100 fmol sample of a five-peptide mixture to which was added 100 fmol of a phosphopeptide. The signal from the phosphopeptide at *m/z* 1574 is indicated by the star. A peak at *m/z* 1476, arising from the neutral loss of 98 Da from the phosphopeptide, is indicated by the asterisk. The power density of the laser pulses ranged ~5–9 × 10^7 W/cm^2. (B) The quadrupole mass analyzer was set to transmit only ions with *m/z* ~1476. (C) Precursor ion spectrum of ions giving rise to the fragment at *m/z* 1476 in the collision induced process. The laser power density was decreased to 1–2 × 10^7 W/cm^2, and the voltage on electrode I was set to −2000 V to induce fragmentation (see text). The only signal detected is the phosphopeptide precursor.

We then set the quadrupole mass filter to transmit only signal of the ion at *m/z* 1475, corresponding to the loss of 98 Da from the phosphopeptide. The window for the selection was ±20 Da. No signal corresponding to the intact phosphopeptide was detected under these conditions (Fig. 13B).

Unfortunately, our current construction of the tandem instrument does not allow us to use separate gases in the trap and in the collision cell, forcing us to use He as a collisional gas. However, He is inefficient for CID, requiring us to use high voltages to induce even a small degree of fragmentation. Thus, we decreased the density of laser radiation to our standard operating value and set the voltage on the electrode I (Fig. 2) to −2000 V to cause fragmentation of the ejected ions. Ions ejected from the trap undergo quick acceleration and then deceleration in the field created by this electrode positioned at the entrance of the quadrupole collision cell (Fig. 2). We detected only the precursor at *m/z* 1574, which gives rise to the characteristic fragment at *m/z* 1475 (Fig. 13C). Despite the low efficiency of fragmentation, we selectively detected only the phosphopeptide in the mixture of non-phosphorylated peptides using the precursor mode of the tandem mass spectrometer. This result confirms the proposed principle for improving the efficiency of the linked scan mode in the mass spectrometer assembled in configuration ion trap-collision cell-mass analyzer.

6. Discussion

We have constructed and tested a prototype tandem mass spectrometer designed to increase the efficiency of linked-scan analysis by factor of 100–1000 over conventional linked-scan instruments. The key to this improvement is elimination of the usual losses connected with the ion selection step, through the use of an ion trap in tandem with a collision cell and a mass analyzer (Fig. 1). Ion traps store and sequentially eject ions during the resonant and/or instability scan. If the ejected ions are fragmented in the collision cell, then the MS/MS analysis is performed on all trapped ion species, without the usual scanning losses.

We reason that not all existing ion traps are suitable for incorporation into the current tandem configuration, and that optimally we need a trap capable of operating with 100–1000-fold more ions than is feasible using a standard 3D ion trap [49]. This requirement for high ion capacity arises from a consideration of the minimum time needed to produce and detect fragments of a given *m/z* slice of the ejected ions. Indeed, if we analyze a 3–4 Da window of ejected ions in a time frame of 1 ms, then to cover 3000–4000 *m/z* range we need 1 s to accomplish this scan. To achieve a duty cycle at least 50%, it is necessary to fill the trap for ~1 s. Current ion sources can readily produce fluxes in the range of 10^6–10^9 ions/s and thus, we need an ion trap that can accommodate a large number of ions.

Despite significant advances in increasing ion capacity of ion traps 30–50-fold [55,56], we still need another factor 10–100 to take a full advantage of the proposed tandem configuration. Our novel high-capacity ion trap can manipulate with 10^6–10^7 ions without significant degradation in its performance. The improvement in the ion capacity is accomplished by decoupling the process of ion storage and ion ejection. While filling in the ion trap, ions are allowed to occupy a large volume along the *z*-axis of the device. When the time for ion ejection comes, ions are compressed towards the center of the ion trap where they are eventually ejected after the ion kinetic energy exceeds the depth of the potential well at the middle, widest part, of the ion trap. Based on purely geometrical considerations we predict a gain of ∼300–500 in ion storage capacity compared with the 3D ion traps, and a gain of ∼10 compared with the linear ion trap [55–57].

Our calculations support the proposed mechanisms of ion storage and ejection. Simulations indicate that the ions migrate between two boundaries of stability that move inwards during the ramping process. The amplitude of ion oscillations around the *z*-axis increases at the boundary of stability and hence increases the force along the *z*-axis that pushes the ions inside the electric field of lesser density. For some period of time, the ions stay inside of the boundaries of stability until the amplitude of the main RF increases enough to compress the ions to the center of the ion trap and consequently eject them. The current model allows us to calculate ion trajectories under a variety of initial conditions.

Our experiments demonstrated that the tandem instrument based on the tapered ion trap is capable of measuring a few femtomole of peptide in a single 1s scan of the instrument. The resolution of the device is 100–450, corresponds to a 10–20 Da width of an ion peak at half maximum. We envisage that the resolution can be increased by introducing several straightforward improvements to the ion trap. For example, our current construction does not support a careful alignment of the small quadrupoles at the central part of the trap as well as the possibility to change the distance between rods to compensate the effects of a field distortion by the slit [55].

We also tested the tandem mass spectrometer for measuring the precursor spectra of ions stored in the trap. Ions are ejected from the trap with average kinetic energy sufficient to overcome the potential barrier of the trap. The choice of the main frequency (here 333 kHz) is important for determining the depth of effective potential well [47]. For example, we estimate that ions at *m*/*z* 1673 leave the ion trap with average kinetic energy ∼100 eV (Fig. 8), Since this ejection energy depends linearly on the *m*/*z* value [47], ions with *m*/*z* 3495 will be ejected with ∼200 eV. This kinetic energy would be optimal to cause efficient dissociation of the ions in the collision cell where it filled with the Nitrogen or Argon gas at the same pressure (∼4 mTorr) [45]. The efficiency of ion dissociation in Helium (our current collision gas) is negligible under these conditions. Unfortunately, our current construction of the tandem instrument does not allow us to use separate gases in the trap and in the collision cell. The yield of ion fragmentation in He gas at 4 mTorr and the field ∼2000 V/cm was very small, in the range of a few percent. Nevertheless, this was sufficient to demonstrate the feasibility of performing ion precursor scans on all ions stored in the trap. Our results indicate that we can selectively detect a phosphopeptide in the mixture of nonphosporylated peptides.

Although we used a quadrupole mass filter as the final stage of the tandem instrument to perform selective scans, other mass analyzers can be used to detect the fragmentation spectra of the ejected ions. The use of a time-of-flight instruments at the last stage has an exquisite advantage of providing the possibility to collect fragmentation spectra of all ions stored in the ion trap [61]. Based on our prototype instrument, we intend to build a fully functional model of such a tandem mass spectrometer for detecting modification sites on proteins and profiling their abundances with unprecedented speed and sensitivity. This new tool should be useful for rapid, sensitive detection and profiling of modification states of proteins.

Acknowledgments

This work was supported by National Institutes of Health Grants RR00862 (BTC), and R21 RR023120 (KAN).

References

[1] R. Uy, F. Wold, Science 198 (1977) 890.
[2] C. Kannicht (Ed.), Posttranslational Modifications of Proteins: Tools for Functional Proteomics, Methods in Molecular Biology, Humana Press, 2002.
[3] S. Westermann, K. Weber, Nat. Rev. Mol. Cell Biol. 4 (2003) 938.
[4] R. Seger, Methods Mol. Biol. Ser. 250 (2004).
[5] W.J. Boyle, P. van der Geer, T. Hunter, Methods Enzymol. 201 (1991) 110.
[6] A.J. Czernik, J.A. Girault, A.C. Nairn, J. Chen, G. Snyder, J. Kebabian, P. Greengard, Methods Enzymol. 201 (1991) 264.
[7] M. Mann, O.N. Jensen, Nat. Biotechnol. 21 (2003) 255.
[8] B.A. Garcia, C.M. Barber, S.B. Hake, C. Ptak, F.B. Turner, S.A. Busby, J. Shabanowitz, R.G. Moran, C.D. Allis, D.F. Hunt, Biochemistry 44 (2005) 13202.
[9] D.J. Harvey, Expert. Rev. Proteomics 2 (2005) 87.
[10] M.R. Larsen, P. Roepstorff, Fresenius J. Anal. Chem. 366 (2000) 677.
[11] B.A. Garcia, J. Shabanowitz, D.F. Hunt, Methods 35 (2005) 256.
[12] M.T. Davis, T.D. Lee, J. Am. Soc. Mass Spectrom. 9 (1998) 194.
[13] D.S. Kirkpatrick, C. Denison, S.P. Gygi, Nat. Cell Biol. 7 (2005) 750.
[14] S.A. Beausoleil, M. Jedrychowski, D. Schwartz, J.E. Elias, J. Villen, J. Li, M.A. Cohn, L.C. Cantley, S.P. Gygi, Proc. Natl. Acad. Sci. U.S.A. 101 (2004) 12130.
[15] M.R. Larsen, T.E. Thingholm, O.N. Jensen, P. Roepstorff, T.J. Jorgensen, Mol. Cell Proteomics 4 (2005) 873.
[16] E.J. Chang, V. Archambault, D.T. McLachlin, A.N. Krutchinsky, B.T. Chait, Anal. Chem. 76 (2004) 4472.
[17] R.A. Yost, C.G. Enke, J. Am. Chem. Soc. 100 (1978) 2274.
[18] D. Zakett, A.E. Schoen, R.W. Kondrat, R.G. Cooks, J. Am. Chem. Soc. 101 (1979) 6781.
[19] R.A. Yost, R.K. Boyd, Methods Enzymol. 193 (1990) 154.
[20] M.J. Cole, C.G. Enke, Anal. Chem. 63 (1991) 1032.
[21] Y. Tondeur, W.N. Niederhut, J.E. Campana, S.R. Missler, Biomed. Environ. Mass Spectrom. 14 (1987) 449.
[22] J.P. Murphy III, R.A. Yost, Rapid Commun. Mass Spectrom. 14 (2000) 270.
[23] J.E. McClellan, S.T. Quarmby, R.A. Yost, Anal. Chem. 74 (2002) 5799.
[24] M.J. Schroeder, J. Shabanowitz, J.C. Schwartz, D.F. Hunt, J.J. Coon, Anal. Chem. 76 (2004) 3590.

[25] K. Sato, T. Asada, M. Ishihara, F. Kunihiro, Y. Kammei, E. Kubota, C.E. Costello, S.A. Martin, H.A. Scoble, K. Biemann, Anal. Chem. 59 (1987) 1652.
[26] K. Beimann, Pure Appl. Chem. 65 (1993) 1021.
[27] R.S. Annan, S.A. Carr, Anal. Chem. 68 (1996) 3413.
[28] J. Qin, B.T. Chait, Anal. Chem. 69 (1997) 4002.
[29] R.D. Ladner, S.A. Carr, M.J. Huddleston, D.E. McNulty, S.J. Caradonna, J. Biol. Chem. 271 (1996) 7752.
[30] R.S. Annan, M.J. Huddleston, R. Verma, R.J. Deshaies, S.A. Carr, Anal. Chem. 73 (2001) 340.
[31] K.R. Jonscher, J.R. Yates III, J. Biol. Chem. 272 (1997) 1735.
[32] H. Steen, M. Fernandez, S. Ghaffari, A. Pandey, M. Mann, Mol. Cell Proteomics 2 (2003) 138.
[33] M.J. Huddleston, M.F. Bean, S.A. Carr, Anal. Chem. 65 (1993) 877.
[34] S.A. Carr, M.J. Huddleston, M.F. Bean, Protein Sci. 2 (1993) 183.
[35] P.A. Haynes, R. Aebersold, Anal. Chem. 72 (2000) 5402.
[36] K.D. Greis, W. Gibson, G.W. Hart, J. Virol. 68 (1994) 8339.
[37] C. Borchers, C.E. Parker, L.J. Deterding, K.B. Tomer, J. Chromatogr. A 854 (1999) 119.
[38] J.Y. Kim, K.W. Kim, H.J. Kwon, D.W. Lee, J. Yoo, Anal. Chem. 74 (2002) 5443.
[39] J. Rappsilber, W.J. Friesen, S. Paushkin, G. Dreyfuss, M. Mann, Anal. Chem. 75 (2003) 3107.
[40] K. Zhang, P.M. Yau, B. Chandrasekhar, R. New, R. Kondrat, B.S. Imai, M.E. Bradbury, Proteomics 4 (2004) 1.
[41] A.S. Petersson, H. Steen, D.E. Kalume, K. Caidahl, P. Roepstorff, J. Mass Spectrom. 36 (2001) 616.
[42] J. Castro-Perez, R. Plumb, L. Liang, E. Yang, Rapid Commun. Mass Spectrom. 19 (2005) 798.
[43] B. Keil, Specificity of Proteolysis, Springer-Verlag KG, Berlin, 1992.
[44] J. Stafford Jr., J. Am. Soc. Mass Spectrom. 13 (2002) 589.
[45] A.N. Krutchinsky, W. Zhang, B.T. Chait, J. Am. Soc. Mass Spectrom. 11 (2000) 493.
[46] A.N. Krutchinsky, M. Kalkum, B.T. Chait, Anal. Chem. 73 (2001) 5066.
[47] P.H. Dawson, in: P.H. Dawson (Ed.), American Vacuum Society Classics, Woodbury, New York, 1995.
[48] R.E. March, R.J. Hughes, Quadrupole Storage Mass Spectrometry, Wiley, New York, 1989.
[49] J.C. Schwartz, Proceedings of the 9th Sanibel Conference on Mass Spectrometry, Sanibel Island, FL, 1997.
[50] F. Vedel, M. Vedel, in: R.E. March, J.F.J. Todd (Eds.), Practical Aspects of Ion Trap Mass Spectrometry, vol. 1, CRC Press, 1995.
[51] A. Mordehai, B. Miller, J. Bai, A. Brekenfeld, C. Baessmann, M. Shubert, K. Hosea, Proceedings of the 52nd ASMS Conference on Mass Spectrometry and Allied Topics, May 23–27, Nashville, TN, 2004.
[52] S.A. Lammert, W.R. Plass, C.V. Thompson, M.B. Wise, Int. J. Mass Spectrom. 212 (2001) 25.
[53] M.E. Bier, J.E.P. Syka, US Patent 5,420,525, May 30, 1995.
[54] Z. Ouyang, G. Wu, Y. Song, H. Li, W.R. Plass, R.G. Cooks, Anal. Chem. 76 (2004) 4595.
[55] J.C. Schwartz, M.W. Senko, J.E.P. Syka, J. Am. Soc. Mass Spectrom. 13 (2002) 659.
[56] J.W. Hager, Rapid Commun. Mass Spectrom. 16 (2002) 512.
[57] D.J. Douglas, A.J. Frank, D. Mao, Mass Spectrom. Rev. 24 (2005) 1.
[58] D. Gerlich, in: C.Y. Ng, M. Baer (Eds.), Advances in Chemical Physics Series, LXXXII, John Wiley & Sons, 1992.
[59] A.N. Krutchinsky, I.V. Chernushevich, V.L. Spicer, W. Ens, K.G. Standing, J. Am. Soc. Mass Spectrom. 9 (1998) 569.
[60] A.N. Krutchinsky, A.V. Loboda, V.L. Spicer, W. Ens, K.G. Standing, Rapid Commun. Mass Spectrom. 12 (1998) 508.
[61] H. Wang, D.S. Kennedy, Y. Zhu, K.D. Nugent, G.K. Taylor, D.R Goodlett, 54th ASMS Conference on Mass Spectrometry and Allied Topics, May 28 – June 1, Seattle, WA, 2006.